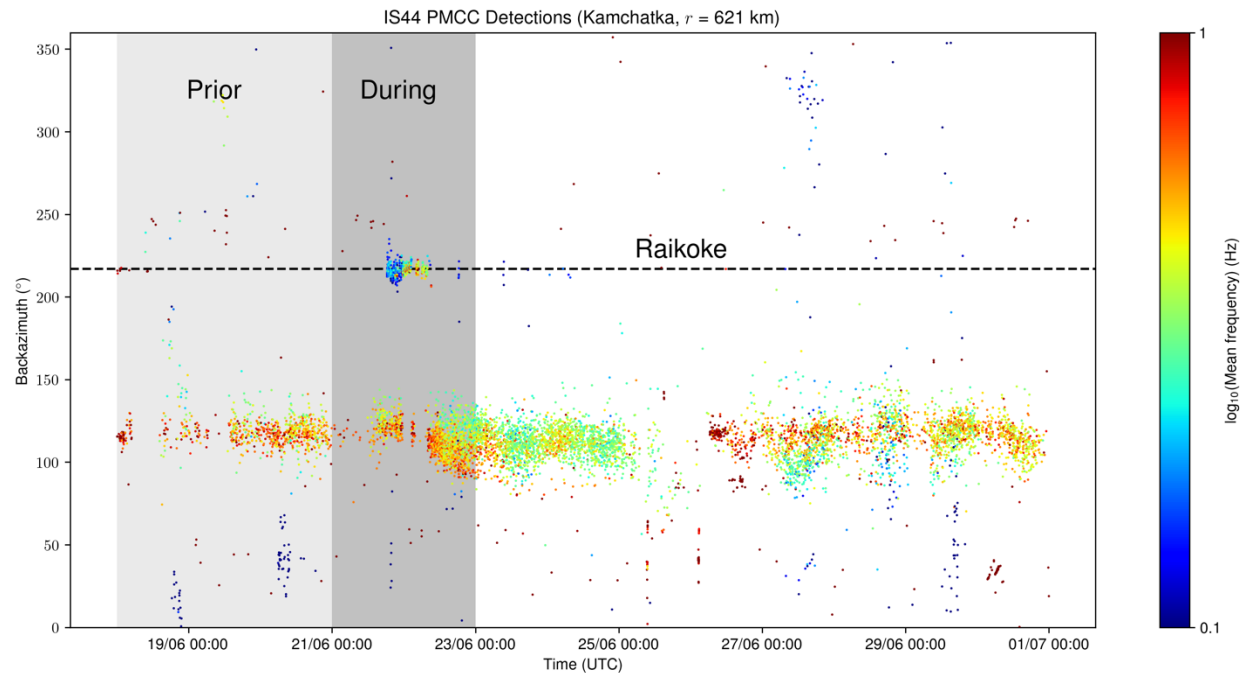


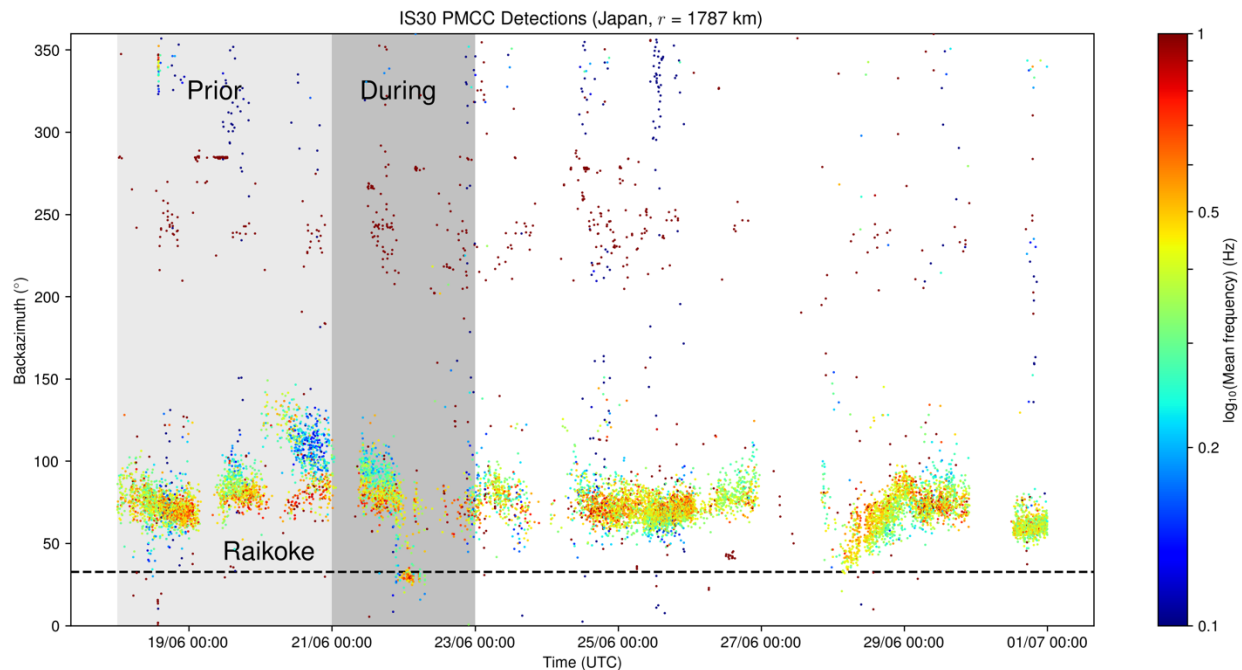
Supporting Figures for: Evaluating the State-of-the-Art in Remote Volcanic Eruption Characterization Part I: Raikoke Volcano, Kuril Islands

Kathleen McKee (0000-0003-3189-9189)¹, Cassandra Smith (0000-0003-2653-4249)², Kevin Reath (0000-0003-1843-8046)³, Eveanjelene Snee (0000-0002-3660-4020)⁴, Sean Maher (0000-0002-9803-916X)⁵, Robin S. Matoza (0000-0003-4001-061X)⁵, Simon Carn (0000-0002-0360-6660)⁶, Larry Mastin (0000-0002-4795-1992)⁷, Kyle Anderson (0000-0001-8041-3996)⁸, David Damby (0000-0002-3238-3961)⁸, Diana Roman (0000-0003-1282-5803)¹, Artem Degterev (0000-0001-6284-8830)⁹, Alexander Rybin (0000-0002-7734-0172)⁹, Marina Chibisova (0000-0003-0677-6945)⁹, Jelle Assink (0000-0002-4990-6845)¹⁰, Rodrigo de Negri Leiva (0000-0003-1283-2579)^{5,11}, Anna Perttu (0000-0003-3590-1549)¹²

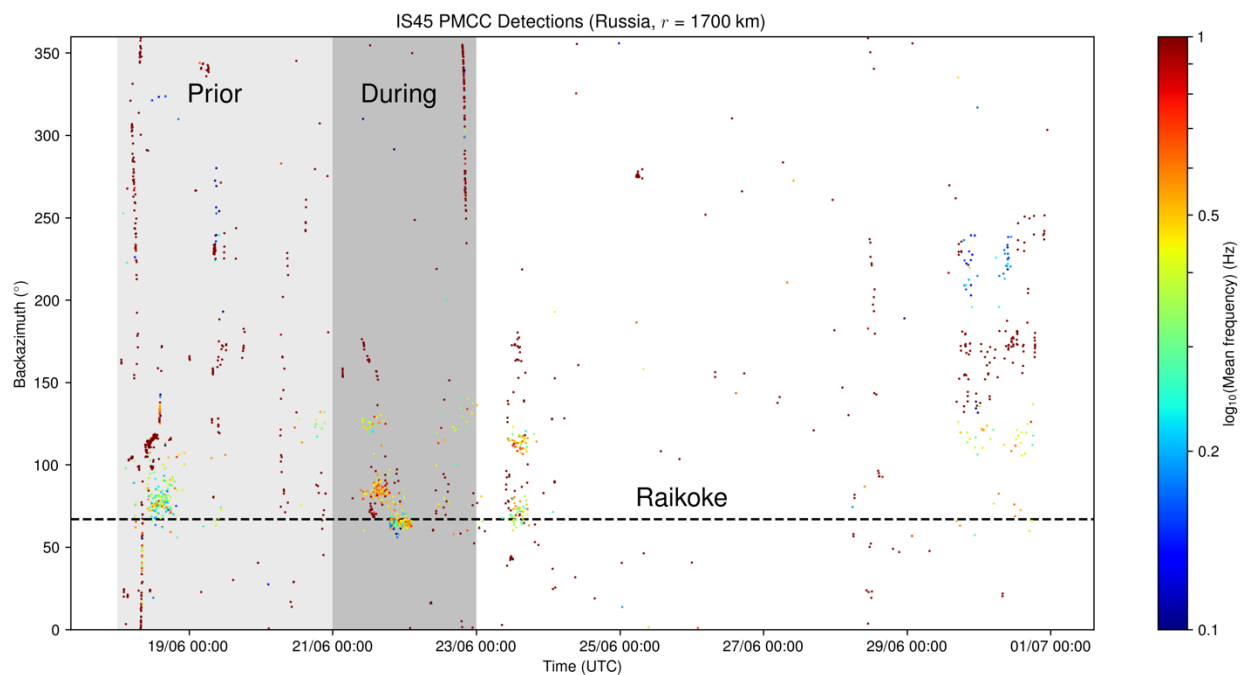
¹Earth and Planets Laboratory, Carnegie Institution for Science, Washington, DC, USA, ²Alaska Volcano Observatory, Anchorage, AK, USA, ³Department of Earth and Atmospheric Sciences, Cornell University, Ithaca, NY, USA, ⁴School of Earth and Ocean Sciences, Cardiff University, Cardiff, Wales, UK, ⁵Department of Earth Science and Earth Research Institute, University of California, Santa Barbara, Santa Barbara, CA, USA, ⁶Department of Geological and Mining Engineering and Sciences, Michigan Technological University, Houghton, MI, USA, ⁷U.S. Geological Survey Cascades Volcano Observatory, Vancouver, WA, USA, ⁸U.S. Geological Survey, California Volcano Observatory, Moffett Field, CA, USA, ⁹Sakhalin Volcanic Eruptions Response Team (SVERT), Institute of Marine Geology and Geophysics, Yuzhno-Sakhalinsk, Russia, ¹⁰R&D Seismology and Acoustics Department, Royal Netherlands Meteorological Institute (KNMI), De Bilt, Netherlands, ¹¹NDC-CTBT of the Chilean Nuclear Energy Commission, Chile, ¹²Earth Observatory of Singapore, Nanyang Technological University, Singapore



Sup. Fig. 1 - PMCC array processing results from IS44 (Kamchatka) for the Raikoke eruption showing the backazimuths of coherent detections over time. Colors represent the mean frequency of the detection. Dashed line at 217° shows the backazimuth to Raikoke volcano. The shaded “During” region (2019-06-21T00:00:00 to 2019-06-23T00:00:00 UTC) represents the time interval used to locate the eruption with IMS_vASC. The shaded “Prior” region (2019-06-18T00:00:00 to 2019-06-21T00:00:00 UTC) represents the time interval used to clean the IMS_vASC grid of detection clutter from ambient noise (see Matoza et al., (2017) for method details).

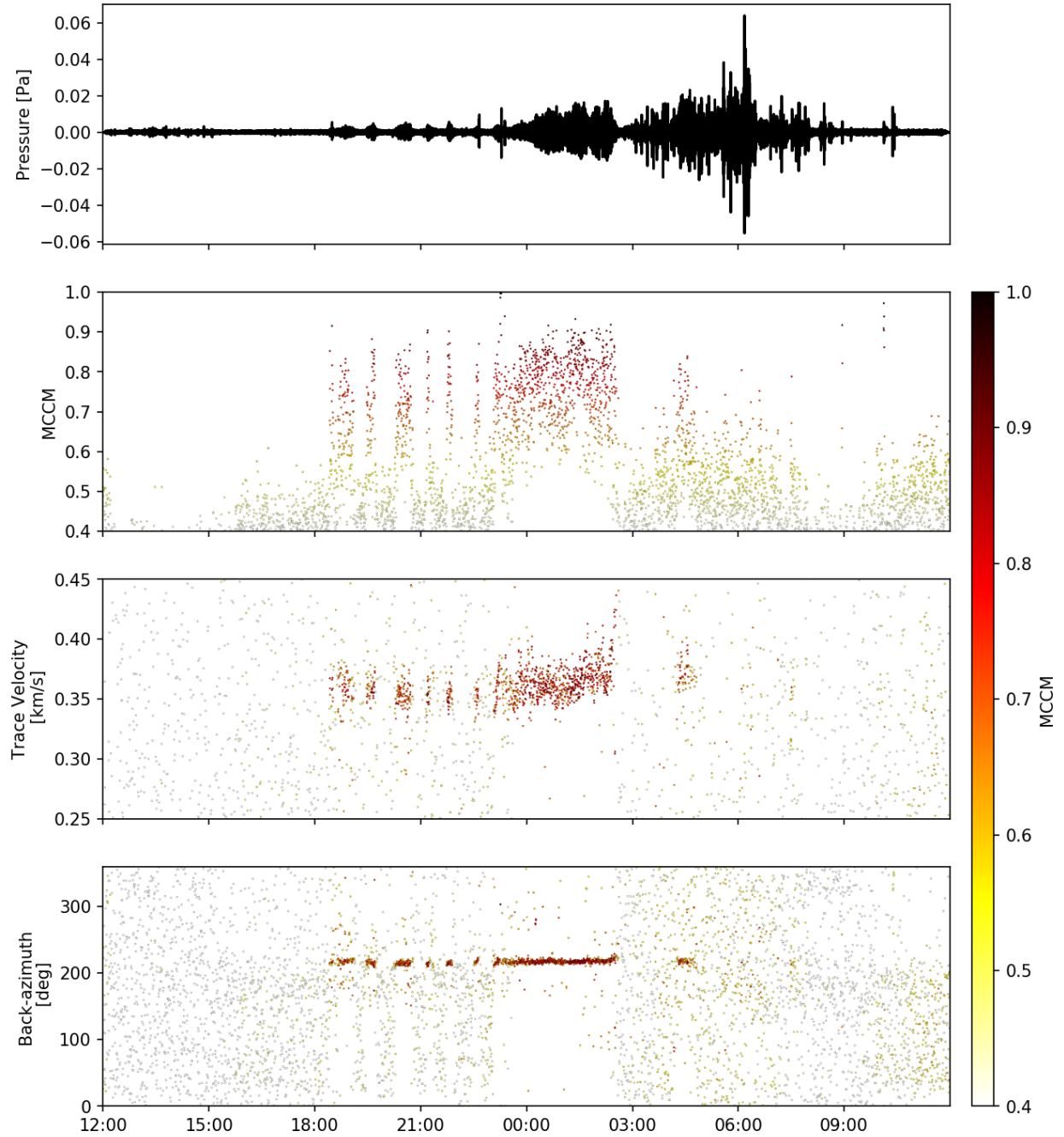


Sup. Fig. 2 - PMCC array processing results from IS30 (Japan) for the Raikoke eruption showing the backazimuths of coherent detections over time. Colors represent the mean frequency of the detection. Dashed line at 33° shows the backazimuth to Raikoke volcano. The shaded “During” region (2019-06-21T00:00:00 to 2019-06-23T00:00:00 UTC) represents the time interval used to locate the eruption with IMS_vASC. The shaded “Prior” region (2019-06-18T00:00:00 to 2019-06-21T00:00:00 UTC) represents the time interval used to clean the IMS_vASC grid of detection clutter from ambient noise (see Matoza et al., (2017) for method details).

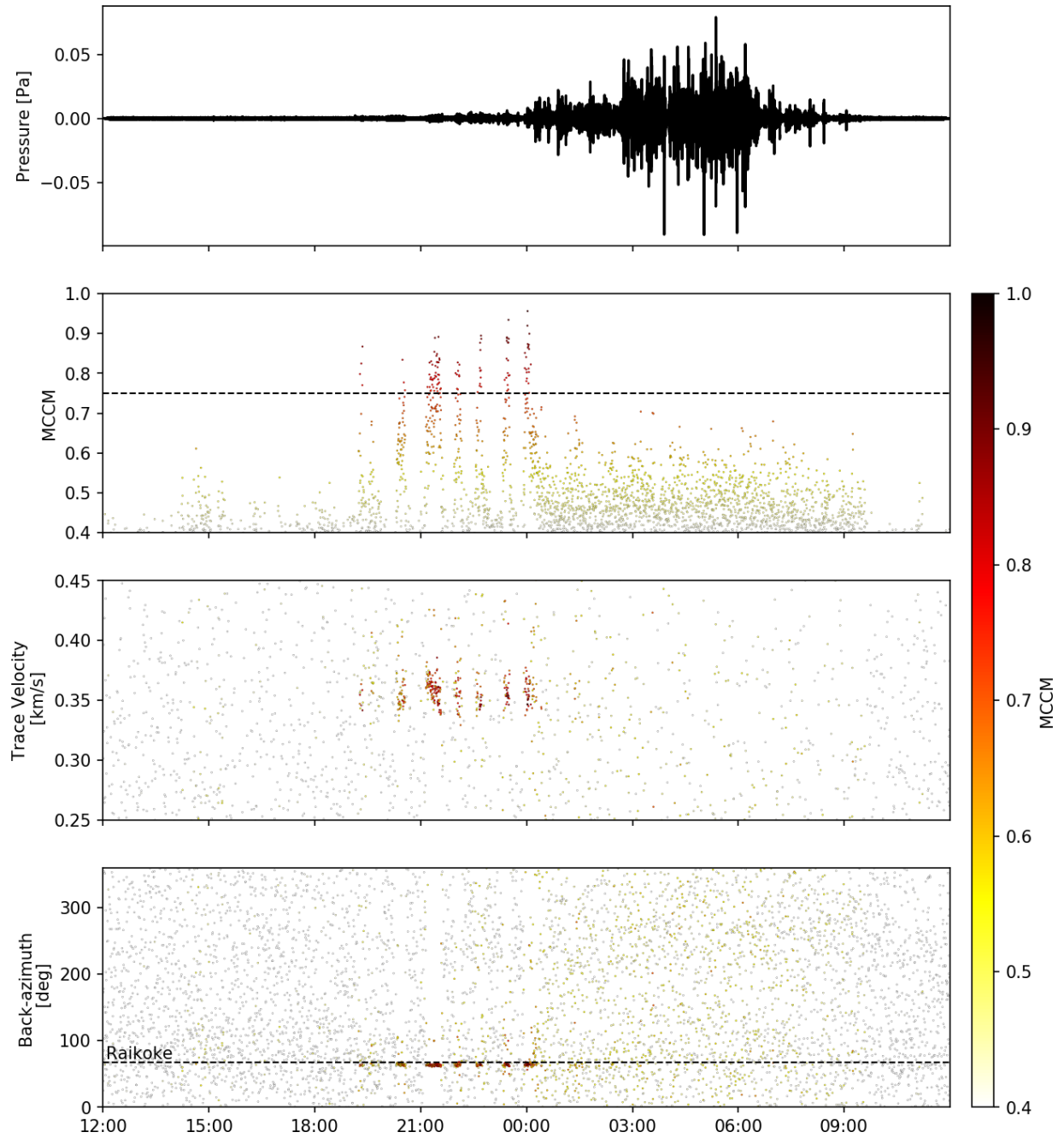


Sup. Fig. 3 - PMCC array processing results from IS45 (Russia) for the Raikoke eruption showing the backazimuths of coherent detections over time. Colors represent the mean frequency of the detection. Dashed line at 67° shows the backazimuth to Raikoke volcano. The shaded “During” region (2019-06-21T00:00:00 to 2019-06-23T00:00:00

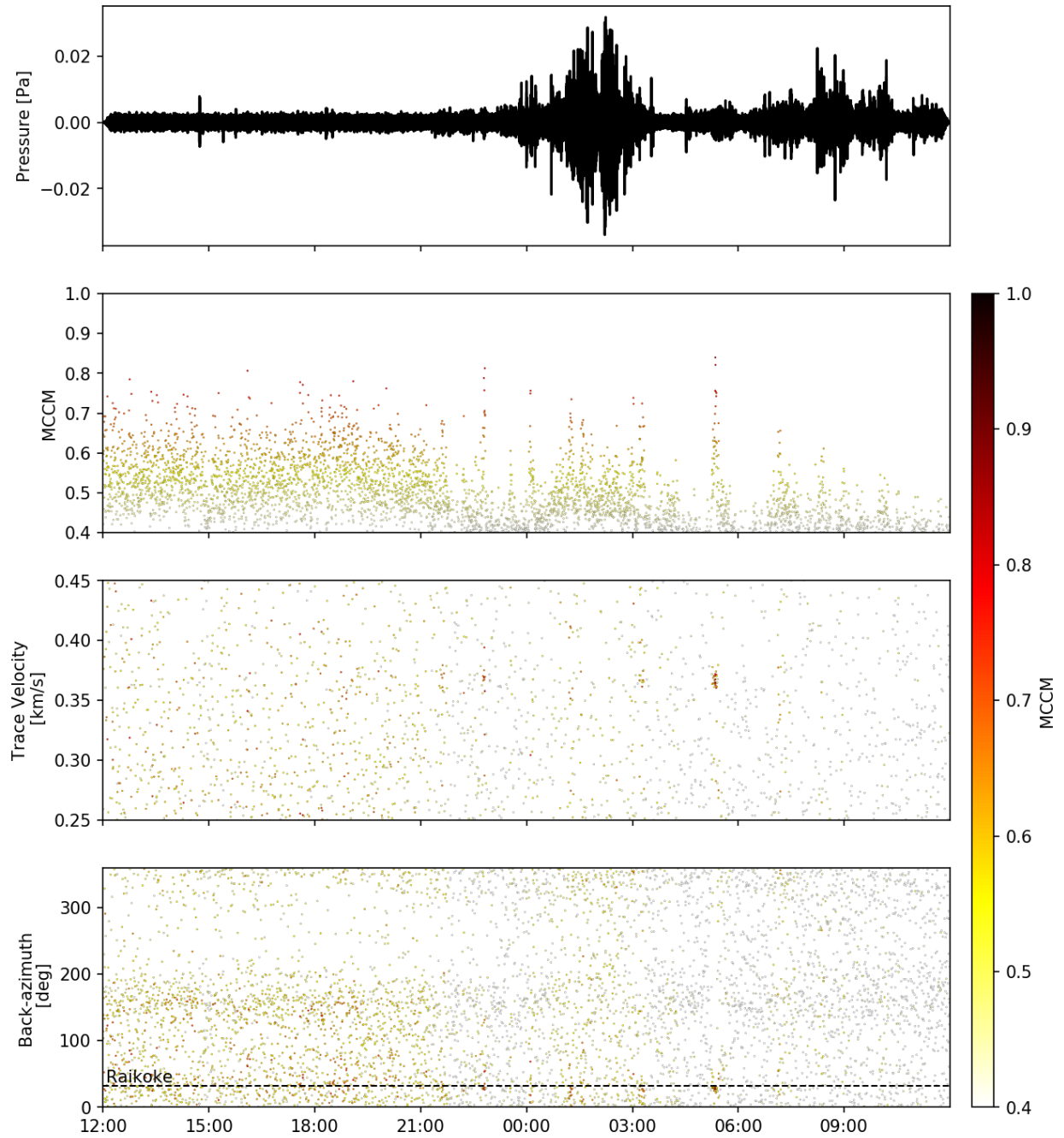
UTC) represents the time interval used to locate the eruption with IMS_vASC. The shaded “Prior” region (2019-06-18T00:00:00 to 2019-06-21T00:00:00 UTC) represents the time interval used to clean the IMS_vASC grid of detection clutter from ambient noise (see Matoza et al., (2017) for method details).



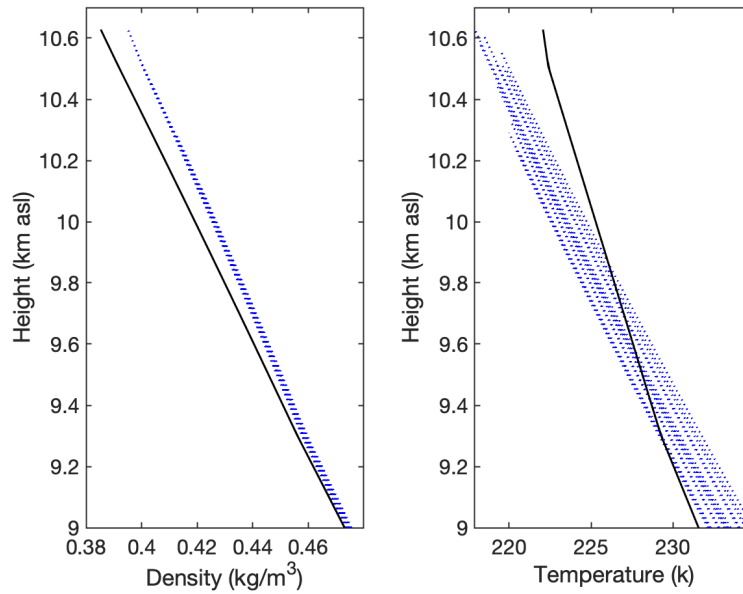
Sup. Fig. 4 - IS44 MdCCM array detection results Raikoke for 21 June at 12:00 to 22 June at 12:00 UTC, data filtered from 0.1 to 5.0 Hz. Top: Best beam of infrasound; 2nd: MCCM, mean cross correlation maximum; 3rd: Estimated trace velocity for each time window; Bottom: Estimated back-azimuth for each time window.



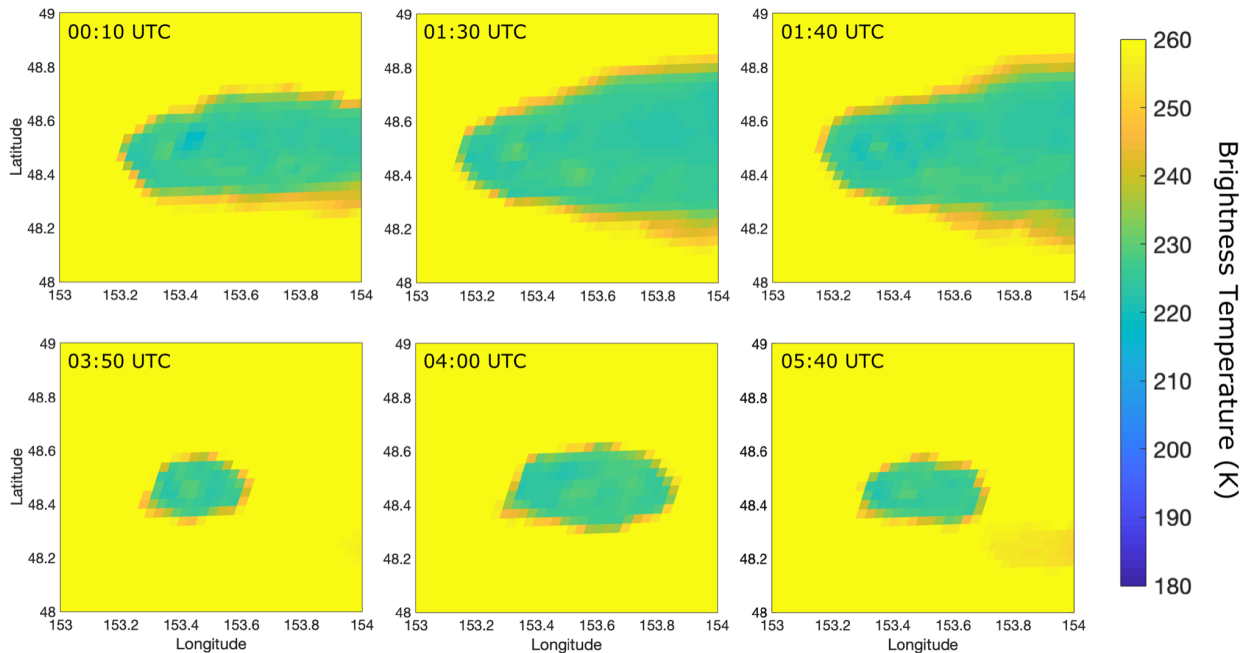
Sup. Fig. 5 - IS45 MdCCM array detection results Raikoke for 21 June at 12:00 to 22 June at 12:00 UTC, data filtered from 0.1 to 5.0 Hz. Top: Best beam of infrasound; 2nd: MCCM, mean cross correlation maximum; 3rd: Estimated trace velocity for each time window; Bottom: Estimated back-azimuth for each time window.



Sup. Fig. 6 - IS30 MdCCM array detection results Raikoke for 21 June at 12:00 to 22 June at 12:00 UTC, data filtered from 0.1 to 5.0 Hz. Top: Best beam of infrasound; 2nd: MCCM, mean cross correlation maximum; 3rd: Estimated trace velocity for each time window; Bottom: Estimated back-azimuth for each time window.



Sup. Fig. 7 - Comparison of plume density profile (left) and temperature (right) in blue with the atmospheric density and temperature profile from ECMWF in black. Multiple model runs are plotted from each run in a Monte-Carlo simulation, where the top modelled plume temperature is within error of the coldest pixel observed by Himawari at 23:20 21/06/2019. This shows that the top of the plume is colder and denser than the surrounding atmosphere above the neutral buoyancy level.



Sup. Fig. 8 - Brightness temperature at wavelength 11 μm images for six times (specific times at top left of each image), where the ash plume potentially reached the stratosphere as the centre of the ash cloud is warmer than the surrounding ash.

Sup. Table 1. Table of the parameter space used to selected the initial source conditions in the Monte Carlo plume modelling

Source Parameter	Explored Range
Velocity (m s^{-1})	25 - 250
Gas Mass Fraction	0.01 - 0.05
Temperature (K)	900 - 1400
Radius (m)	1 - 150